Article

Not peer-reviewed version

Phase Structures, Electromechanical Responses and Electrocaloric Effects in K0.5Na0.5NbO3 Epitaxial Film Controlled by Non-Isometric Misfit Strain

Yingying Wu , Yun Ou * , Jinlin Peng , Chihou Lei *

Posted Date: 10 August 2023

doi: 10.20944/preprints202308.0839.v1

Keywords: non-equiaxed misfit strain; K0.5Na0.5NbO3; Electrocaloric effect; Ferroelectric thin films

Article

Phase Structures, Electromechanical Responses and Electrocaloric Effects in K0.5Na0.5NbO3 Epitaxial Film Controlled by Non-Isometric Misfit Strain

Yingying Wu [1,$], Yun Ou [2,*,$], Jinlin Peng [3] and Chihou Lei [4,*]

[1] School of Materials Science and Engineering, Hunan University of Science and Technology, Xiangtan 411201, China
[2] Hunan Provincial Key Laboratory of Health Maintenance for Mechanical Equipment, Hunan University of Science and Technology, Xiangtan 411201, China
[3] All-Solid-State Energy Storage Materials and Devices Key Laboratory of Hunan Province, College of Information and Electronic Engineering, Hunan City University, Yiyang 413002, China
[4] Department of Aerospace and Mechanical Engineering, Saint Louis University, Saint Louis, Missouri 63103-1110, USA
* Correspondence: ouyun101@hnust.edu.cn (Y.Ou.); chihou.lei@slu.edu (C.Lei.)
$ Co-Authors: This author equally to this work

Abstract: Environmentally friendly lead-free K1-xNaxNbO3 (KNN) ceramics possess electromechanical properties comparable to lead-based ferroelectric materials, but cannot meet the needs of device miniaturization, and the corresponding thin films lack of theoretical and experimental studies. To this end, we developed the nonlinear phenomenological theory for ferroelectric materials to study the effects of non-equiaxed misfit strain on the phase structure, electromechanical properties and electrical response of K0.5Na0.5NbO3 epitaxial films and constructed the in-plane misfit strain (-) -phase diagrams. The results show that K0.5Na0.5NbO3 epitaxial film under non-equiaxed in-plane strain can exhibit abundant phase structures, including orthorhombic and phases, tetragonal and phases, and monoclinic phases. Moreover, in the vicinity of -, - and - phase boundaries, K0.5Na0.5NbO3 epitaxial films exhibit excellent dielectric constant, while at - and - phase boundaries large piezoelectric coefficient is observed. It was also found that high permittivity and piezoelectric coefficients exist near the -, - and - phase boundaries due to the existence of polymorphic phase boundaries (PPB) in the KNN system, which makes it easy to polarize near the phase boundaries, and the polarizability changes suddenly, leading to electromechanical enhancement. In addition, the results show that the K0.5Na0.5NbO3 thin films possess a large electrocaloric response at the phase boundary at the phase boundaries. And the maximum adiabatic temperature change is about 3.62 K when the electric field change is 30 MV/m at room temperature, which is significantly enhanced compared with equiaxed strain. This study provides theoretical guidance for obtaining K1-xNaxNbO3 epitaxial thin films with excellent properties.

Keywords: non-equiaxed misfit strain; $K_{0.5}Na_{0.5}NbO_3$; Electrocaloric effect; Ferroelectric thin films

1. Introduction

Ferroelectric materials own electromechanical coupling properties due to the existence of spontaneous polarization [1,2], and have been widely used in electronic components such as capacitors, memories, actuators, etc [3,4]. $Pb(Zr_xTi_{1-x})O_3$ (PZT) ceramics is one of the most widely studied ferroelectric materials [5,6] which possesses excellent performance due to their polymorphic phase boundaries (PPB). The phase structure changes suddenly near the morphotropic phase boundary (MPB) leading to enhanced electromechanical response. However, lead-based ceramics is harmful to our human health and environment [7–10]. Therefore, the research and development of lead-free piezoelectric materials have become the general trend.

In 2004, Saito et al. firstly prepared $K_{1-x}Na_xNbO_3$ (KNN) textured ceramics with excellent piezoelectric properties ($d_{33} = 416$ pC/N) near the O-T phase boundary, and then reported that modified and highly textured KNN-based lead-free piezoelectric ceramics possess high piezoelectric coefficient reaching $500 \sim 700 pC/N$, equivalent to those in PZT [11,12]. KNN-based will be a very promising lead-free ferroelectric material, and it is the best substitute for PZT materials, which has aroused extensive interest of researchers.

Over the past years, researchers have studied the composition and the resulting performance of bulk KNN materials, and found that there is a great correlation between the phase boundary and the electromechanical performance [13–16]. Wang et al. designed the a new phase boundary coexisting tetragonal and rhombohedral phase in 2014 and found that the KNN-based ceramics near the phase boundary have excellent piezoelectric properties [17]. It is generally believed that the enhancement mechanism of tetragonal and rhombohedral phase boundary of KNN base is similar to the morphotropic phase boundary [18,19].

In recent years, with the rapid development of high-level integrated circuits, KNN-based bulk ceramics have been unable to meet the needs of device miniaturization [3,20]. However, there are few studies for high-performance KNN-based thin films. The theoretical exploration of thin films, such as the influence of misfit strain on its phase structure, electromechanical properties and electrocaloric performance are rarely reported, which makes the preparation lack of theoretical guidance.

Compared with the bulk structures, due to the constraints of the boundary conditions imposed in thin films, the film lattice does not match between the substrate and the film, resulting in in-plane misfit strain. It is well known that misfitmisfit strain can affect the phase structure of ferroelectric thin films [21], which can further affect the electromechanical properties and electrical response of thin films [22,23]. So it can be seen that misfit strain can effectively regulate the physical properties of ferroelectric thin films [24]. Currently, Bai et al. [25] studied the effect of misfit strain on the phase structure and electromechanical properties of KNN thin films grown on cubic substrates under different compositions. Zhou et al. [26] studied the phase transition of KNN films under an external electric field through thermodynamic theoretical calculations, but they focused on the influence of extrinsic properties on the film. However, for common KNN films grown on non-cubic substrates subjected to an in-plane non-equiaxed misfit strain, the correlations between the intrinsic phase structure, electromechanical and electrocaloric properties are lacking.

Using nonlinear thermodynamic theory, we construct the in-plane misfit strain phase diagram and study the effects of non-equiaxed in-plane biaxial misfit strain on the phase structure, intrinsic electromechanical properties and electrocaloric response of $K_{0.5}Na_{0.5}NbO_3$ epitaxial films at room temperature. It provides some theoretical guidance for optimizing the performance and experimental preparation of $K_{1-x}Na_xNbO_3$ thin films.

2. Theoretical Method

2.1. Thermodynamic Potential and Electromechanical Properties of Epitaxial Thin Films

Following the Landau-Devonshire theory applied to ferroelectric bulk at room temperature [27], conventional orthogonal coordinate systems with axes x_1 along [100], x_2 along [010] and x_3 along [001] are selected as reference. The free energy density of ferroelectric bulk grown along (001) orientation can be described by a polynomials in polarization $p_i \left(i = 1,2,3\right)$ and stress $\sigma_i \left(i = 1,2,...6\right)$, which is expressed in Voigt notation as [28]:

Preprints (www.preprints.org) | NOT PEER-REVIEWED | Posted: 10 August 2023 doi:10.20944/preprints202308.0839.v1

$$
\begin{aligned}
G = {} & a_1\left(p_1^2+p_2^2+p_3^2\right)+a_{11}\left(p_1^4+p_2^4+p_3^4\right)+a_{12}\left(p_1^2p_2^2+p_1^2p_3^2+p_2^2p_3^2\right)+\\
& a_{111}\left(p_1^6+p_2^6+p_3^6\right)+\alpha_{123}\left(p_1p_2p_3\right)^2+\alpha_{111}(p_1^6+p_2^6+p_3^6)+\\
& \alpha_{1111}(p_1^8+p_2^8+p_3^8)+\alpha_{1112}[p_3^2\,(p_1^6+p_2^6)+p_2^2\,(p_1^6+p_3^6)+p_1^2\,(p_3^6+p_2^6)]+\\
& \alpha_{112}[p_3^2(p_1^4+p_2^4)+p_2^2(p_1^4+p_3^4)+p_1^2(p_3^4+p_2^4)]+\\
& \alpha_{1122}(p_1^4p_2^4+p_1^4p_3^4+p_3^4p_2^4)+\alpha_{1123}[p_1^4p_2^2p_3^2+p_1^2p_2^4p_3^2+p_1^2p_2^2p_3^4]-\\
& \frac{1}{2}S_{11}\left(\sigma_1^2+\sigma_2^2+\sigma_3^2\right)-S_{12}\left(\sigma_1\sigma_2+\sigma_1\sigma_3+\sigma_2\sigma_3\right)-\frac{1}{2}S_{44}\left(\sigma_4^2+\sigma_5^2+\sigma_6^2\right)-\\
& Q_{11}\left(\sigma_1p_1^2+\sigma_2p_2^2+\sigma_3p_3^2\right)-Q_{44}\left(\sigma_4p_2p_3+\sigma_5p_1p_3+\sigma_6p_1p_2\right)-\\
& Q_{12}\left[\sigma_1\left(p_2^2+p_3^2\right)+\sigma_2\left(p_1^2+p_3^2\right)+\sigma_3\left(p_2^2+p_1^2\right)\right]-p_1E_1-p_2E_2-p_3E_3
\end{aligned}
\tag{1}
$$

where $E_I\left(I=1,2,3\right)$ are the components of external electric fields; a_1, a_{ij} and a_{ijk} are thedielectric coefficients; S_{ij} are the elastic compliance coefficients; Q_{ij} are the electrostrictive coefficients. Moreover, the first dielectric coefficient a_1 is influenced by temperature via:

$$
a_1=\frac{T-T_C}{2\varepsilon_0 C} \tag{2}
$$

where C is the Curie constant, ε_0 is the vacuum dielectric constant and T_C is the Curie temperature of the involved material.

For thin films that are treated under the configuration of plane stress, assume the top surface is traction-free, then $\sigma_3=\sigma_4=\sigma_5=0$. Assume that the $K_{1-x}Na_xNbO_3$ epitaxial film grown on anisotropic substrate are subjected to non-equal in-plane misfit axial strain [29], that is $u_1\neq u_2$, with zero shear strain component ($u_6=0$).

The Gibbs free energy of ferroelectric thin film can then be obtained by using Legendre transformation [30], that is $\tilde{G}=G+u_1\sigma_1+u_2\sigma_2$, with $u_i=-\partial G/\partial\sigma_i$. For instance, the thermodynamic potential $\tilde{G}$ for $K_{1-x}Na_xNbO_3$ epitaxial films can be expressed by [29,30]:

$$
\begin{aligned}
\tilde{G} = {} & \alpha_1^*p_1^2+\alpha_2^*p_2^2+\alpha_{11}^*\left(p_1^4+p_2^4\right)+\alpha_{12}^*\left(p_1p_2\right)^2+\alpha_{13}^*P_3^2\left(p_1^2+p_2^2\right)\\
& +\alpha_3^*p_3^2+\alpha_{12}^*\left(p_1p_2\right)^2+\alpha_{13}^*p_3^2\left(p_1^2+p_2^2\right)+\alpha_3^*p_3^2+\alpha_{33}^*p_3^4\\
& +\alpha_{123}\left(p_1p_2p_3\right)^2+\alpha_{111}(p_1^6+p_2^6+p_3^6)+\alpha_{1111}(p_1^8+p_2^8+p_3^8)\\
& +\alpha_{1112}[p_3^2\,(p_1^6+p_2^6)+p_2^2\,(p_1^6+p_3^6)+p_1^2\,(p_3^6+p_2^6)]\\
& +\alpha_{112}[p_3^2(p_1^4+p_2^4)+p_2^2(p_1^4+p_3^4)+p_1^2(p_3^4+p_2^4)]\\
& +\alpha_{1122}(p_1^4p_2^4+p_1^4p_3^4+p_3^4p_2^4)+\alpha_{1123}[p_1^4p_2^2p_3^2+p_1^2p_2^4p_3^2+p_1^2p_2^2p_3^4]\\
& +\frac{(u_1^2+u_2^2)S_{11}-2S_{12}u_1u_2}{2(S_{11}^2-S_{12}^2)}-E_3p_3-E_2p_2-E_1p_1
\end{aligned}
\tag{3}
$$

where

Preprints (www.preprints.org) | NOT PEER-REVIEWED | Posted: 10 August 2023 doi:10.20944/preprints202308.0839.v1

$$\alpha_1^* = \alpha_1 - \frac{u_1\left(Q_{11}S_{11} - Q_{12}S_{12}\right) + u_2\left(Q_{12}S_{11} - Q_{11}S_{12}\right)}{S_{11}^2 - S_{12}^2} \tag{4}$$

$$\alpha_2^* = \alpha_1 - \frac{u_2\left(Q_{11}S_{11} - Q_{12}S_{12}\right) + u_1\left(Q_{12}S_{11} - Q_{11}S_{12}\right)}{S_{11}^2 - S_{12}^2} \tag{5}$$

$$\alpha_3^* = \alpha_1 - \frac{Q_{12}\left(u_1 + u_2\right)}{S_{11} + S_{12}} \tag{6}$$

$$\alpha_{11}^* = \alpha_{11} + \frac{S_{11}\left(Q_{11}^2 + Q_{12}^2\right) - 2Q_{11}Q_{12}S_{12}}{2\left(S_{11}^2 - S_{12}^2\right)} \tag{7}$$

$$\alpha_{33}^* = \alpha_{11} + \frac{Q_{12}^2}{S_{11} + S_{12}} \tag{8}$$

$$\alpha_{12}^* = \alpha_{12} - \frac{S_{12}\left(Q_{11}^2 + Q_{12}^2\right) - 2Q_{11}Q_{12}S_{11}}{2\left(S_{11}^2 - S_{12}^2\right)} + \frac{Q_{44}^2}{2S_{44}} \tag{9}$$

$$\alpha_{13}^* = \alpha_{12} + \frac{Q_{12}\left(Q_{11} + Q_{12}\right)}{S_{11} + S_{12}} \tag{10}$$

Here, α_i^* and α_{ij}^* refer to the normalized dielectric constants. The material-specific coefficients (parameters) are listed on Table 1.

Based on the principle of minimum energy, the polarization components of the thin films at equilibrium (stable phase) can be computed as [31]:

$$\frac{\partial \tilde{G}}{\partial p_1} = 0, \qquad \frac{\partial \tilde{G}}{\partial p_2} = 0, \qquad \frac{\partial \tilde{G}}{\partial p_3} = 0 \tag{11}$$

From the computed polarization components $(p_1,\ p_2,\ p_3)$, the relative dielectric constants of the ferroelectric thin films are obtained as [32,33]:

$$\varepsilon_{ij} = 1 + \eta_{ij} / \varepsilon_0 \tag{12}$$

where

$$\eta = \chi^{-1} = \begin{pmatrix} \frac{\partial^2 \tilde{G}}{\partial p_1 \partial p_1} & \frac{\partial^2 \tilde{G}}{\partial p_1 \partial p_2} & \frac{\partial^2 \tilde{G}}{\partial p_1 \partial p_3} \\ \frac{\partial^2 \tilde{G}}{\partial p_2 \partial p_1} & \frac{\partial^2 \tilde{G}}{\partial p_2 \partial p_2} & \frac{\partial^2 \tilde{G}}{\partial p_2 \partial p_3} \\ \frac{\partial^2 \tilde{G}}{\partial p_3 \partial p_1} & \frac{\partial^2 \tilde{G}}{\partial p_3 \partial p_2} & \frac{\partial^2 \tilde{G}}{\partial p_3 \partial p_3} \end{pmatrix}^{-1} \tag{13}$$

The piezoelectric coefficient d_{in} for the (001) orientation is calculated by [34]:

Preprints (www.preprints.org) | NOT PEER-REVIEWED | Posted: 10 August 2023 doi:10.20944/preprints202308.0839.v1

$$d_{in} = \frac{\partial s_n}{\partial p_1}\eta_{i1} + \frac{\partial s_n}{\partial p_2}\eta_{i2} + \frac{\partial s_n}{\partial p_3}\eta_{i3} \tag{14}$$

In this work, the piezoelectric coefficients d_{15} and d_{33} will be analyzed. The in-plane normal strain s_3 and shear strain s_5 are derived [33]:

$$s_3 = \frac{2u_m S_{12}}{S_{11}+S_{12}} + [Q_{12} - \frac{S_{12}(Q_{11}+Q_{12})}{S_{11}+S_{12}}(p_1^2+p_2^2) + (Q_{11} - \frac{2S_{12}Q_{12}}{S_{11}+S_{12}})p_3^2] \tag{15}$$

$$s_5 = Q_{44}p_1p_3 \tag{16}$$

Table 1. Coefficients used in the computation for $K_{0.5}Na_{0.5}NbO_3$ thin films, where T represents the temperature at K [27,35,36].

Coeff	Values	Units
α_1	$4.29\times10^7 \times[\mathrm{Coth}(140/T) - \mathrm{Coth}(140/657)]$	$C^{-2}m^2N$
α_{11}	-2.7302×10^8	$C^{-4}m^6N$
α_{12}	1.0861×10^9	$C^{-4}m^6N$
α_{111}	3.0448×10^9	$C^{-6}m^{10}N$
α_{112}	-2.7270×10^9	$C^{-6}m^{10}N$
α_{123}	1.5513×10^{10}	$C^{-6}m^{10}N$
α_{1111}	2.4044×10^{10}	$C^{-8}m^{14}N$
α_{1112}	3.7328×10^9	$C^{-8}m^{14}N$
α_{1122}	3.3485×10^{10}	$C^{-8}m^{14}N$
α_{1123}	-6.2017×10^{10}	$C^{-8}m^{14}N$
Q_{11}	0.16	m^4/C^2
Q_{12}	–0.072	m^4/C^2
Q_{44}	0.084	m^4/C^2
S_{11}	5.57×10^{-12}	m^2/N
S_{12}	-1.57×10^{-12}	m^2/N
S_{44}	13.1×10^{-12}	m^2/N
C_{latt}	1.485×10^6	J/m^3K

2.2. Electrocaloric Effect Temperature Change

Electrocaloric effect refers to the phenomenon of temperature change caused by external electric field or entropy change caused by isothermal conditions of dielectric materials under adiabatic conditions [37,38]. Based on the principle of entropy conservation, the isothermal entropy change ΔS and adiabatic temperature change ΔT can be computed to characterize the electrocaloric

Preprints (www.preprints.org) | NOT PEER-REVIEWED | Posted: 10 August 2023 doi:10.20944/preprints202308.0839.v1

performance of ferroelectric thin films. For instance, the system isothermal entropy change S_{total} is the sum of dipole entropy S_{dip} and lattice entropy S_{latt}, that is [22,39],

$$S_{total}(E,T)=S_{dip}(E,T)+S_{latt}(T) \tag{17}$$

where the dipole entropy is attributed to the electric dipole in the film, and it is a function of the polarization P_i, which is related to the applied electric field, while the lattice entropy depends on temperature and is independent of the applied electric field.

$$S_{dip}(E,T)=-\left(\frac{\tilde{\partial}G(E,T)}{\partial T}\right)_E \tag{18}$$

$$dS_{latt}(T)=\frac{C_{latt}}{T}dT \tag{19}$$

where C_{latt} is the heat capacity per unit volume of the thin film. During the electrocaloric process, the total entropy of the system remains zero under adiabatic electric field; T_i and T_f denote the initial temperature and the final temperature respectively; E_i and E_f represent the initial electric field and the final electric field, respectively.

$$dS=dS_{dip}+dS_{latt}=0 \tag{20}$$

$$\Delta S_{latt}=S_{latt}(T_f)-S_{latt}(T_i)=C_{latt}\int_{T_i}^{T_f}\frac{1}{T}dT\approx C_{latt}(T_i)In\left(\frac{T_f}{T_i}\right) \tag{21}$$

$$\Delta S_{dip}=S_{dip}(E_f,T_f)-S_{dip}(E_i,T_i)=\frac{\partial\tilde{G}(E_i,T_i)}{\partial T}-\frac{\partial\tilde{G}(E_f,T_f)}{\partial T} \tag{22}$$

The final temperature of the material can be calculated from the formula:

$$T_f=T_i exp\left\{-\frac{1}{C_{latt}}\left[\frac{\partial\tilde{G}(E_i,T_i)}{\partial T}-\frac{\partial\tilde{G}(E_i,T_i)}{\partial T}\right]\right\} \tag{23}$$

Moreover, the expression of the final adiabatic temperature change can be written as [40–42]:

$$\Delta T=T_f-T_i=T_i exp\left\{-\frac{1}{C_{latt}}\left[\frac{\partial\tilde{G}(E_i,T_i)}{\partial T}-\frac{\partial\tilde{G}(E_i,T_i)}{\partial T}\right]\right\}-T_i, \tag{24}$$

3. Results and Analysis

The nonlinear thermodynamic model is applied to study the phase structure, electromechanical properties and electrocaloric response of $K_{0.5}Na_{0.5}NbO_3$ epitaxial film at room temperature under non-equiaxed in-plane misfit strain. The correlation coefficients used in the calculation are shown in Table 1. With these parameters and the nonlinear thermodynamic model, the phase structure and dielectric properties of $K_{0.5}Na_{0.5}NbO_3$ bulk material were accurately repeated [27], indicating that the calculated parameters are reliable. For instance, at 25°C, when the equiaxed compressive strain gradually transforms to tensile strain, the phase structure of the $K_{0.5}Na_{0.5}NbO_3$ film changes with the routes

Preprints (www.preprints.org) | NOT PEER-REVIEWED | Posted: 10 August 2023 doi:10.20944/preprints202308.0839.v1

$c \to r_{11} \to a_1a_1$, which is consistent with the phase structure corresponding to the phase diagram (u_1 - u_2) along the diagonal line [26], which also validate the correctness of the calculation results

First, we studied the effect of non-equiaxed in-plane misfit strain on the phase structure of $K_{0.5}Na_{0.5}NbO_3$ epitaxial film at room temperature (25°C), and constructed the phase diagram over in-plane strains u_1 - u_2, as shown in Figure 1a, and the corresponding changes in the polarization components are shown in Figure 1b–d.

When subjected to equiaxed misfit strain, the phase structure corresponds to the diagonal line of the phase diagram in Figure 1a. It can be found that when the equiaxed compressive strain gradually transforms to tensile strain, the phase structure of $K_{0.5}Na_{0.5}NbO_3$ film changes sequentially as $c \to r_{11} \to a_1a_1$, which is consistent with the literature results, as shown in Figure 2a [26], which shows the correctness of the calculation results.

Interestingly, when u_1 and u_2 are not equal, which corresponds to in-plane non-equiaxed misfit strain, the symmetry of the phase structure of the $K_{0.5}Na_{0.5}NbO_3$ thin film is obviously broken at room temperature leading to the emergence of rich variety of phase structures. There are seven phase structures according to the applied misfit strains, and the polarization characteristics of each phase are featured in Table 2.

Among these phases, the monoclinic phase corresponds to the center of the phase diagram, and other phases are distributed around it. The pattern of the overall phase diagram is symmetric about the line $u_1 = u_2$. The tetragonal phase exists in the region subjected to larger compressive in-plane strain. It can be seen from Figure 1b that in the transition from compressive strain to tensile strain, the plane polarization component p_3 gradually decreases to zero, making the c-phase disappear.

At the same time, $u_1 \neq u_2$ induces $p_1 \neq p_2$, leading unequal energies of the two phases a_1c and a_2c. The a_2c-phase is more likely to form in the region with $u_2 > 0$, while a_1c-phase is more likely to form in the region $u_1 > 0$. At the same time, the tetragonal a_2 phase is located in the region in the phase diagram with large tensile normal strain u_2, while the a_1 phase exists in the region with large tensile normal strain u_1. The a_1a_2-phase is located in the region with large tensile normal strains u_1 and u_2.

From the diagram showing polarization components, it can be seen that the non-equiaxed in-plane misfit strains u_1 and u_2 can affect the polarization of the film at room temperature. Figure 1b indicates that the in-plane polarization increases with the increase of the tensile strain u_1, Figure 1c indicates that the change of direction of polarization p_2 is parallel to the strain u_2 and becomes larger as it increases, while Figure 1d shows that the out-of-plane polarization p_3 exists stably in the region with compressive strain and increases with the increase of compressive strains u_1 and u_2.

Preprints (www.preprints.org) | NOT PEER-REVIEWED | Posted: 10 August 2023 doi:10.20944/preprints202308.0839.v1

Table 2. Phase structures and characteristic polarization components of $K_{0.5}Na_{0.5}NbO_3$ thin films at room temperature and under no electric field.

Phase	Polarization
c	$p_1 = p_2 = 0, p_3 \neq 0$
a_1	$p_1 \neq 0, p_2 = p_3 = 0$
a_2	$p_2 \neq 0, p_1 = p_3 = 0$
a_1c	$p_1 \neq p_3 \neq 0, p_2 = 0$
a_2c	$p_2 \neq p_3 \neq 0, p_1 = 0$
a_1a_1	$p_1 = p_2 \neq 0, p_3 = 0$
a_1a_2	$p_1 > p_2 \neq 0, p_3 = 0$ / $p_2 > p_1 \neq 0, p_3 = 0$
r_{11}	$p_1 = p_2 \neq 0, p_3 \neq 0$
r_{12}	$p_1 \neq p_2 \neq p_3 \neq 0, p_1 > p_2$ / $p_1 \neq p_2 \neq p_3 \neq 0, p_2 > p_1$

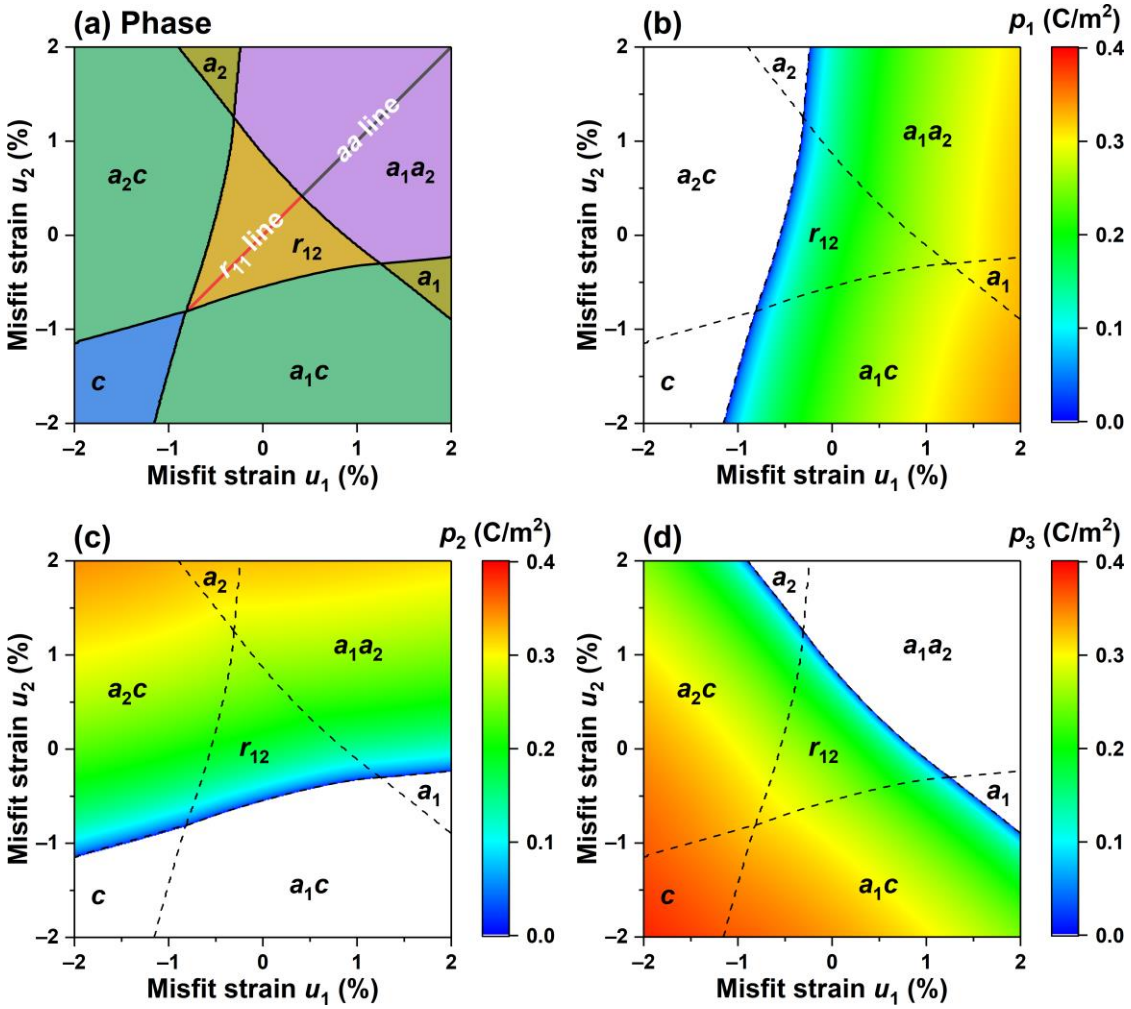

Figure 1. (**a**) Non-isometric misfit strain-strain Phase diagram for $K_{0.5}Na_{0.5}NbO_3$ thin films at 25°C without external electric field; (**b–d**) Pseudo-color maps on strained phase diagrams depicting respectively the polarization components p_1、p_2、p_3.

Next we observe the change of the polarization component with the misfit strain where the conditions with room temperature and no applied electric field are imposed. Figure 2b–d depict the

 doi:10.20944/preprints202308.0839.v1

relationships between polarization components and strains at $u_1 = -1\%$, $u_1 = 0$ and $u_1 = 1.5\%$ respectively.

It is found that in Figure 2b, at $u_1 = -0.01$, as the misfit strain u_2 increases from compressive strain to tensile strain (-2%~2%), the film undergoes a sequence of phase transitions $a_1c \to c \to a_2c$, and the orthorhombic phase accounts for the majority, of which the polarization components p_1 and p_2 experience a sudden change in the $a_1c - c$ phase, while the polarization component p_3 decreases continuously with the increase of strain. As observed in Figure 2c, at $u_1 = 0$, the tetragonal phase degenerates while the monoclinic r_{12} -phase emerges, and the strain u_2 of a_1c phase boundary extended to -0.55% . As the strain u_1 becomes tensile and as the misfit strain u_2 increases, the thin films undergo a sequence of phase transformations $a_1c \to a_1 \to a_1a_2$, the polarization component p_1 has no obvious change, but the abrupt change point of the polarization component p_3 has dropped to the region with compressive strain. Figures 1 and 2 illustrate that, compared with the equiaxed misfit strain, the non-equiaxed misfit strain causes a change in the symmetry of the phase structure, thus inducing a rich variety of phase structures. Moreover, there co-exists multiple phases near the phase boundary leading to easy polarization which enhance the performance, which serve as the mechanism for effective control of the electromechanical properties of $K_{0.5}Na_{0.5}NbO_3$ epitaxial film.

Preprints (www.preprints.org) | NOT PEER-REVIEWED | Posted: 10 August 2023 doi:10.20944/preprints202308.0839.v1

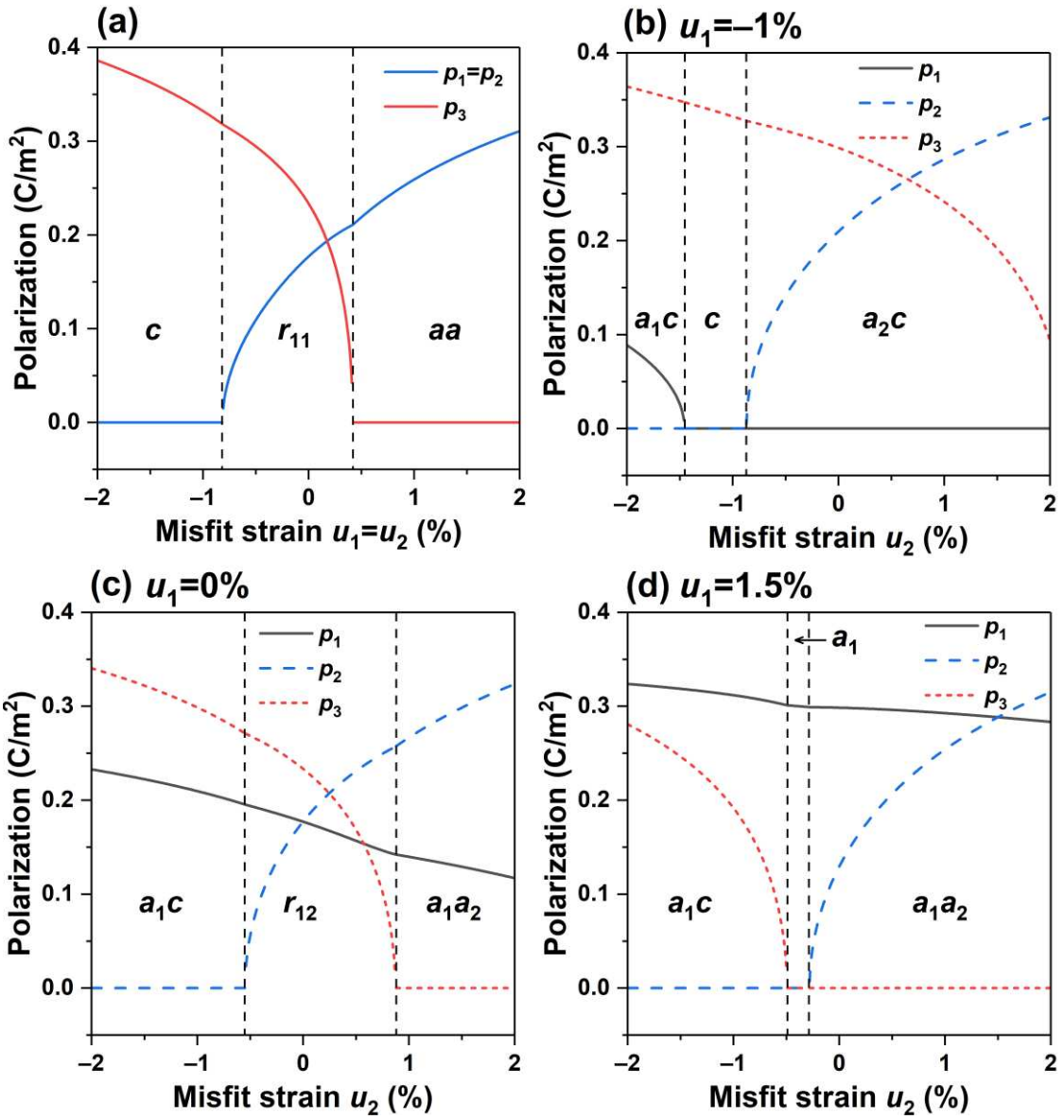

Figure 2. (**a**) Strain-Polarization diagram with $u_1 = u_2$ at 25℃ and subjected to no electric field. Strain u_2 -Polarization diagram with $u_1 \neq u_2$ at 25℃ and subjected to no electric field: $u_1 = -1\%$ (**b**), $u_1 = 0\%$ (**c**), $u_1 = 1.5\%$.

In order to explore the influence of non-equiaxed misfit strain on the electromechanical properties of $K_{0.5}Na_{0.5}NbO_3$ epitaxial film, we calculated the dielectric constant ε_{ij} and piezoelectric coefficient d_{ij} of $K_{0.5}Na_{0.5}NbO_3$ epitaxial film under non-equiaxed misfit strain, as shown in Figures 3–5.

Figure 3a–c shows the stack distribution of the dielectric constants ε_{11}、ε_{22}、ε_{33} on the phase diagram when the non-equiaxed misfit strain (u_1、u_2) interacts at room temperature. Figure 3a demonstrates that near the $c-a_1c$、a_2c-r_{12}、$a_2-a_1a_2$ phase boundary exhibits excellent transverse permittivity ε_{11}, mainly due to the polarization component p_1 gradually decreasing to 0 as the strain u_1 decreases, as shown in Figure 1b. In Figure 3b, the scores of permittivity ε_{22} are

Preprints (www.preprints.org) | NOT PEER-REVIEWED | Posted: 10 August 2023 doi:10.20944/preprints202308.0839.v1

mainly distributed near the multi-phase boundary $c-a_2c$、a_1c-r_{12}、$a_1-a_1a_2$, in the range of low compressive strain u_2.In the region of Figure 3c with a larger tensile strain u_1, application of u_2 induces large ε_{33}, indicating that non-equiaxed misfit strain enhances the dielectric constant near the phase boundaries with the coexistence of multi-phase at room temperature, which is consistent with the discovery in the KNN-based thin film by Lou et al. [43] where a monoclinic phase emerges at room temperature with an obvious performance enhancement near the phase boundary.

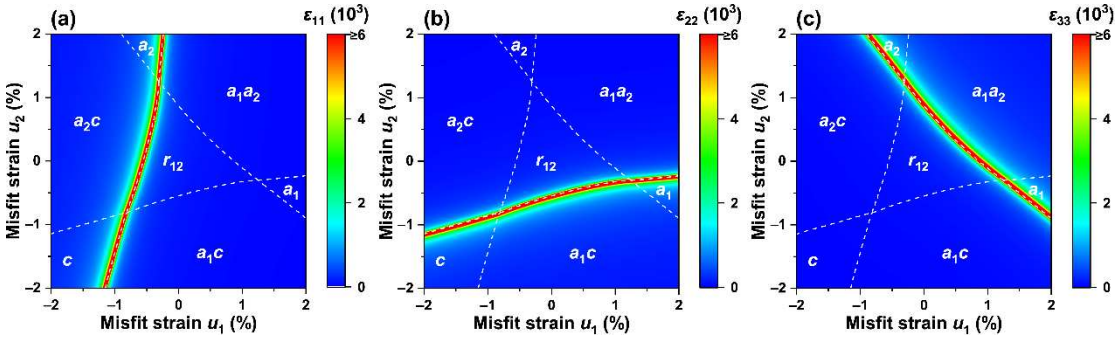

Figure 3. The permittivity (**a**) ε_{11}, (**b**) ε_{22}, (**c**) ε_{33} on strain-strain phase diagram at 25℃ and subjected to an electric field of 0MV/m.

In order to further understand the influence of non-equiaxed strain on the dielectric properties, we selected the region of the phase diagram with high dielectric property to study the relationship between specific strain and polarization characteristics and electromechanical properties, as shown in Figure 4a–c. Figure 4a shows the relationship between the dielectric constant ε_{11}、ε_{22}、ε_{33} and the in-plane strain u_2, when $u_1=-0.01$. Recall that the relationship between the corresponding polarization and the phase structure has been described in Figure 2b. In the figure, it can be seen that with the increase of strain u_2, the dielectric constant ε_{33} increases slowly, and there is no obvious change near the phase boundary, mainly because the out-of-plane polarization component p_3 of the film remains relatively stable when the strain is applied. However, in the region of the phase diagram corresponding to the coexistence of the orthogonal and tetragonal phases, the lateral permittivity ε_{11} and ε_{22} exhibit peak values, when the applied strains are u_2 = -1.44% and $u_2=0.88\%$ respectively. A stable region with a permittivity ε_{11} of about 500 is also observed in the a_2c phase.

For the case with $u_1=0$, when the applied electric field is 0, at 25°C, the phase diagram corresponding to its polarization component is shown in Figure 2c, and a sharp peak of the permittivity appears near the a_1c-r_{12} phase boundary, which can be seen as the abrupt change of the polarization component from Figure 1c. In addition, at this phase transition point, the in-plane polarization p_2 gradually decreases to 0, and its slope changes discontinuously. At the same time, the dielectric constant ε_{33} is located at the point where the slope of the out-of-plane polarization p_3 decreases, and due to the small decrease in the in-plane polarization p_1, the dielectric constant remains basically unchanged, and can maintain good stability at room temperature, and the peak value of ε_{33} throughout the process is greater than ε_{22}.

We also calculated the relationship between dielectric constant and strain as shown in Figure 4c when the tensile strain is $u_1=0.015$. Similar to Figure 4b, phase enhancement effect is also

Preprints (www.preprints.org) | NOT PEER-REVIEWED | Posted: 10 August 2023 doi:10.20944/preprints202308.0839.v1

observed. The peaks of ε_{22} and ε_{33} are located at the orthogonal and tetragonal phase boundaries, and the strain difference between these peaks is small, which is related to the sudden change of the corresponding polarization component, where the discontinuity of ε_{33} is shifted towards the direction of compressive strain ε_{33}.

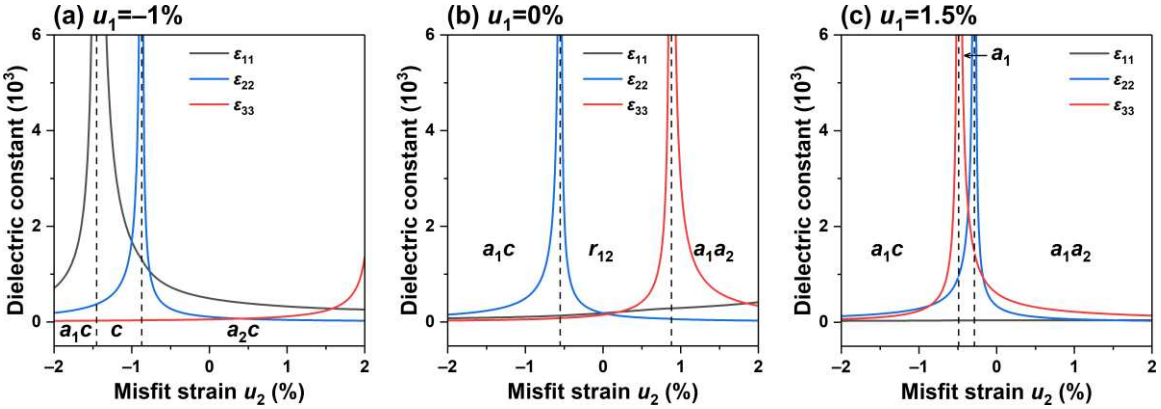

Figure 4. Dielectric constants ε_{ij} as a function of in-plane strain u_2 at 25°C with electric field is 0 MV/): (**a**) $u_1 = -1\%$ (**a**); (**b**) $u_1 = 0\%$ (**b**); (**c**) $u_1 = 1.5\%$.

Next, we studied the influences of non-equiaxed misfit strain on the piezoelectric coefficients d_{15} and d_{33} of the $K_{0.5}Na_{0.5}NbO_3$ epitaxial film. Figure 5a,b shows the cloud distribution of the piezoelectric coefficients d_{15} and d_{33} when the applied electric field is 0 at room temperature. It can be found that the piezoelectric coefficients are all 0 across the phase structures a_2, a_1a_2 and a_1, which is mainly attributed to the distribution of polarization components p_3 in Figure 1d, which is consistent with the piezoelectric coefficients only when the asymmetric structure is met.

The distribution of the extreme value of the piezoelectric coefficient d_{15} is similar to that of the dielectric constant ε_{11}, which exists at the phase boundary of $c - a_1c$ and $a_2c - r_{12}$. The distribution of piezoelectric coefficient d_{33} is similar to the dielectric constant ε_{33} follow similar trend, which undergo enhancement when the polarization component p_3 experiences suddenly change. While it is most well known in the PZT film, which has tetragonal and rhombohedral phases coexisting at MPB, but there is a certain difference in the mechanism of the two. MPB is due to the polarization reversal generated by the material itself, which causes the enhancement effect, and the polarization component will change discontinuously near the phase boundary. For the KNN film, it is regulated by external strain.

Preprints (www.preprints.org) | NOT PEER-REVIEWED | Posted: 10 August 2023 doi:10.20944/preprints202308.0839.v1

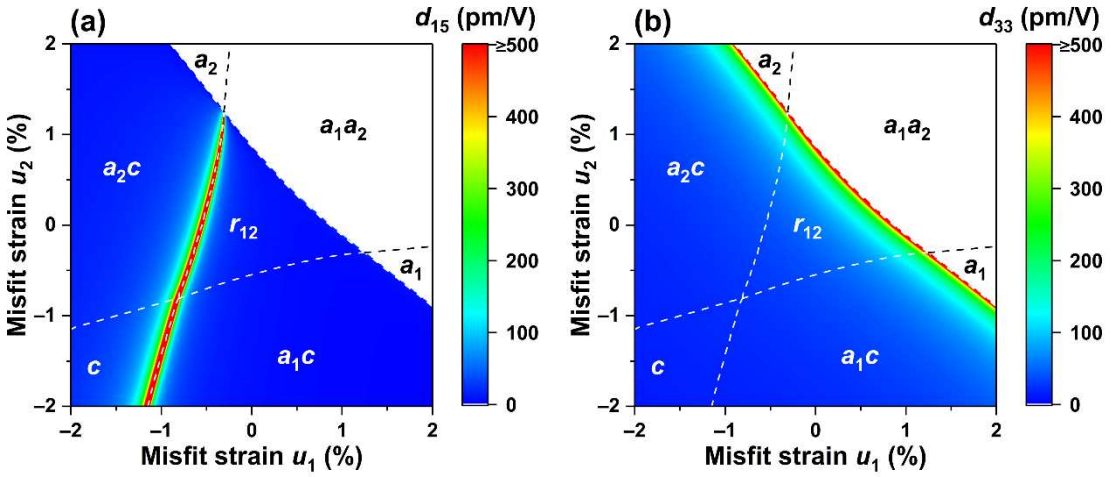

Figure 5. Pseudo-color maps of piezoelectric coefficients on strained phase diagrams at 25°C subjected to no electric field (0MV/m); (**a**) d_{15} (**b**) d_{33}.

In Figure 6a when $u_1 = -0.01$, the relationship between the piezoelectric coefficient and the misfit strain u_1 when it is changed from compressive strain to tensile strain, the phase structure undergoes a transformation: $a_1c \to c \to a_2c$. It is found that the piezoelectric coefficient d_{15} attains a peak value near the $a_1c - c$ phase boundary, and the strain $u_2 = -1.44\%$ is mainly caused by the sharp change of the slope of in-plane polarization p_1. d_{15} is rising continuously. Along the diagonal region of the phase diagram, the influence of phase boundary on the electromechanical performance is minimal, because the polarization components at the phase transition point are all continuously changing with no sudden change in the slope.

Figure 6b,c show the relationship curves of piezoelectric coefficient and strain u_2 when the misfit strain u_1 is 0 and 1.5%, respectively. It can be seen the piezoelectric coefficient d_{15} is almost close to 0 with no obvious change as the polarization in the phase diagram where the polarization component p_1 is in a stable state. When the misfit strain u_1 is not present, the piezoelectric coefficient attains peak values near the $r_{12} - a_1a_2$ phase boundary, while away from the peak, it changes slowly in the orthorhombic a_1c phase. When it is subjected to tensile strain u_1, the piezoelectric coefficient d_{33} peaks at $a_1c - a_1$, which is similar to the dielectric constant ε_{33} because its value is the product of the polarization component and the dielectric constant.

In general, the enhancement of electromechanical properties often occurs near the O-M, O-T, and T-M phase boundaries, which is consistent with the existence of morphotropic phase boundaries in the KNN system and is regulated by external strain. At the same time, when the in-plane polarization p_1 changes suddenly, the dielectric constants ε_{11} and piezoelectric coefficient d_{15} attain peak values, and when the in-plane polarization p_2 changes, the dielectric constants ε_{22} follows the change. When the dielectric constants ε_{33} and piezoelectric coefficient d_{33} are at peaks, the slope of the out-of-plane polarization p_3 often changes abruptly, and when the value of p_3 is 0, the piezoelectric coefficients d_{15} and d_{33} are both zero. By adjusting the magnitude of the misfit strain, the position of the polymorphic phase boundary at room temperature can be controlled, thereby adjusting the electromechanical properties of the thin film system.

Preprints (www.preprints.org) | NOT PEER-REVIEWED | Posted: 10 August 2023 doi:10.20944/preprints202308.0839.v1

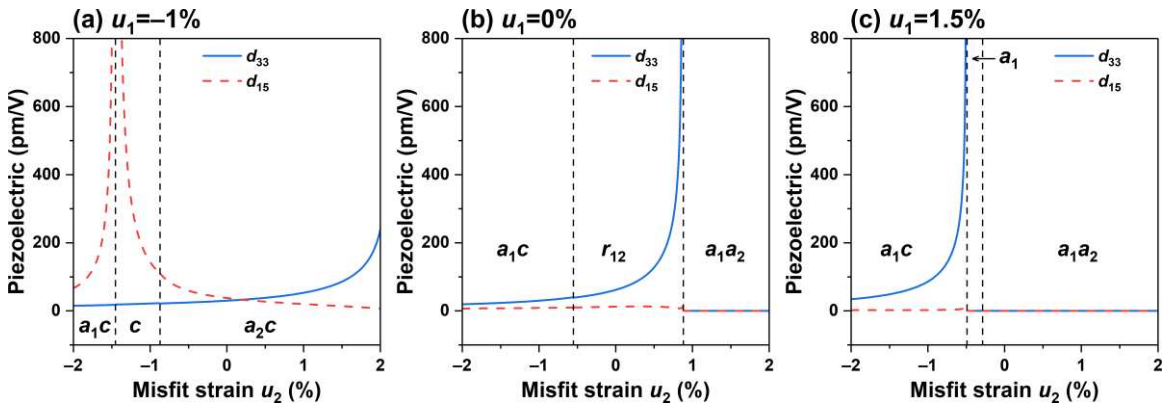

Figure 6. Relation between piezoelectric coefficients and in-plane strain at 25°C and subjected to no electric field (0MV/m) for (**a**) $u_1 = -1\%$; (**b**) $u_1 = 0\%$; (**c**) $u_1 = 1.5\%$.

Finally, we studied the effect of non-equiaxed misfit strain on the adiabatic temperature change ΔT in the electrocaloric response of $K_{0.5}Na_{0.5}NbO_3$ thin film. The results are shown in Figure 5a. At room temperature, an electric field change ΔE of 20MV/m along the [001] direction is applied from an initial electric field of 1 MV/m. The results show that at room temperature the phase boundaries a_1a_2 - r_{12}, a_2c - u_2 and a_1c - u_1 shift towards tensile strain compared to the case with no applied electric field (as indicated by the white dotted line versus phase boundary enhancement), which is due to the applied electric field along the direction of the out-of-plane polarization p_3, leading to enhancement. At the same time, large adiabatic temperature changes appear near the a_1a_2 - r_{12}, a_2c - u_2 and a_1c - u_1 phase boundaries, because the polarization p_3 near these phase boundaries is zero when there is no external electric field, as shown in Figure 1d; when an external electric field in the [001] direction is applied, p_3 increases, causing a large entropy change, resulting in a large adiabatic temperature change ΔT.

There is a difference from the extreme value of the adiabatic temperature change near the ferroelectric phase, indicating that the enhancement is not caused by the Curie temperature of the ferroelectric material, and when the strain u_2 remains constant, enhancement of phase boundaries in Figure 5a shows an upward trend with the increase of the in-plane strain u_1, which may be due to the continuous decrease of the polarization p_3 under this condition. To further understand the electrocaloric effect under the applied electric field and the in-plane misfit, we calculated the characteristics of the adiabatic temperature change with the misfit strain under different applied electric fields when u_1 and u_2 were 0.02 and -0.0045, respectively, as shown in Figure 4b,c. The study found that with the increase of the applied electric field, ΔT increases and remains unchanged upon reaching the peak value. In figure (b), as u1 increases, the adiabatic temperature change shows an upward trend. When u_1 is about -0.7%, ΔT experience a small mutation, which is caused by the emergence of the polarization component p_1. In Figure (c), the adiabatic temperature change can reach 3.62K at $\Delta E = 30\mathrm{MV/m}$, which is further improved compared to the equiaxed misfit strain, and the peak of ΔT is clearly seen at the phase transition in Figure 4c, indicating that an appropriate non-equiaxed misfit strain and an applied electric field can enhance the electrocaloric effect at room temperature. This provides certain guiding significance for the stable operation of the electrocaloric refrigeration device at room temperature.

Preprints (www.preprints.org) | NOT PEER-REVIEWED | Posted: 10 August 2023 doi:10.20944/preprints202308.0839.v1

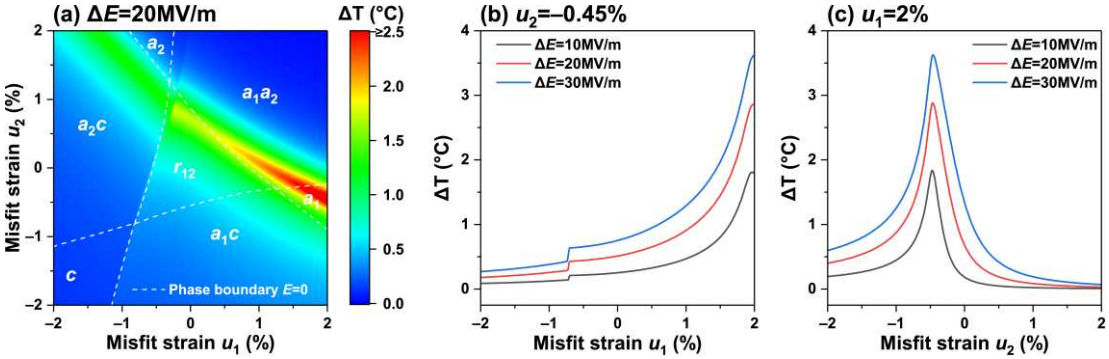

Figure 7. (**a**) Adiabatic temperature change on the strain phase diagram (red line) at 25°C and electric field of $\Delta E = 20$ MV/m. (**b**,**c**) Adiabatic temperature diagram when the electric field is applied at 10, 20, 30MV/m for in-plane misfit strain u_2 of (**b**) 0.45%; (**c**) 2%.

4. Conclusion

In summary, this particle uses the nonlinear Landau-Devonshire thermodynamic theory to study the effects of non-equiaxed in-plane misfit strain on the phase structure, electromechanical properties and electrocaloric effect of $K_{0.5}Na_{0.5}NbO_3$ epitaxial thin films grown on anisotropic substrates at room temperature. It is found that at room temperature, misfit strain can induce orthorhombic phases (a_1a_1、a_1a_2、a_1c、a_2c), tetragonal phases (c、a_1、a_2), and monoclinic phases (r_{11}、r_{12}). Due to the sudden change in the slope of the in-plane and out-of-plane polarization components, the electromechanical properties and electrocaloric effects near the O-M, T-M, and O-T phase boundaries are enhanced. And the phase boundary generated by strain engineering is different from MPB in classical PZT. Among these phase structures, there are excellent dielectric constant ε_{11} and piezoelectric coefficient d_{15} near the a_1c - $_c$ phase boundary. At the same time, the applied electric field along the $[001]$ direction can make the $a_1c - a_1$ phase boundary shift to the direction of strain increase. When the electric field changes to 30MV/m, the adiabatic temperature change ΔT can reach about 3.6K when the film is in the monoclinic phase r_{11}. This work provides some theoretical guidance for the experimental research on the control of lead-free $K_{1-x}Na_xNbO_3$ thin films by strain engineering.

Author Contributions: Y.W.: analysis of the data and review. Y.O.: conceptualization, theoretical calculations, and writing the original draft. J.P.: review, editing, and interpretation of the analyzed data. C.L.: Analysis of data, review, and editing. All authors have read and agreed to the published version of the manuscript.

Funding: This work was partially supported by the National Natural Science Foundation of China (11702092), and the project was supported by the Hunan Provincial Natural Science Foundation of China (2020JJ5182).

Institutional Review Board Statement: Not applicable.

Informed Consent Statement: Not applicable.

Data Availability Statement: Not applicable.

Conflicts of Interest: The authors declare no conflict of interest.

References

1. Liu, Y.; Seidel, J.; Li, J. Multiferroics under the Tip: Probing Magnetoelectric Coupling at the Nanoscale. *National Science Review* **2019**, *6*, 626–628, doi:10.1093/nsr/nwz056.
2. Jiang, P.; Huang, B.; Wei, L.; Yan, F.; Huang, X.; Li, Y.; Xie, S.; Pan, K.; Liu, Y.; Li, J. Resolving Fine Electromechanical Structure of Collagen Fibrils via Sequential Excitation Piezoresponse Force Microscopy. *Nanotechnology* **2019**, *30*, 205703, doi:10.1088/1361-6528/ab0340.

3. Martin, L.W.; Rappe, A.M. Thin-Film Ferroelectric Materials and Their Applications. *Nat Rev Mater* **2016**, *2*, 16087, doi:10.1038/natrevmats.2016.87.
4. Liu, Y.; Li, J. Multiferroics: Looking Back and Going Forward. *Sci. China Technol. Sci.* **2020**, *63*, 2735–2736, doi:10.1007/s11431-020-1742-7.
5. Chen, X.; Xu, S.; Yao, N.; Shi, Y. 1.6 V Nanogenerator for Mechanical Energy Harvesting Using PZT Nanofibers. *Nano Lett.* **2010**, *10*, 2133–2137, doi:10.1021/nl100812k.
6. Zhu, Q.; Pan, K.; Xie, S.; Liu, Y.; Li, J. Nanomechanics of Multiferroic Composite Nanofibers via Local Excitation Piezoresponse Force Microscopy. *Journal of the Mechanics and Physics of Solids* **2019**, *126*, 76–86, doi:10.1016/j.jmps.2019.02.005.
7. Li, J.F.; Wang, K.; Zhu, F.Y.; Cheng, L.Q.; Yao, F.Z. (K,Na)NbO_3 -Based Lead-Free Piezoceramics: Fundamental Aspects, Processing Technologies, and Remaining Challenges. *J. Am. Ceram. Soc.* **2013**, *96*, 3677–3696, doi:10.1111/jace.12715.
8. Carl, K.; Härdtl, K.H. On the Origin of the Maximum in the Electromechanical Activity in Pb(Zr_xTi_{1-x})O_3 Ceramies near the Morphotropic Phase Boundary. *Phys. Stat. Sol. (a)* **1971**, *8*, 87–98, doi:10.1002/pssa.2210080108.
9. Auciello, O.; Gifford, K.D.; Lichtenwalner, D.J.; Dat, R.; Al-Shareef, H.N.; Bellur, Kashyap.R.; Kincon, A.I. A Review of Composition-Structure-Property Relationships for PZT-Based Heterostructure Capacitors. *Integrated Ferroelectrics* **1995**, *6*, 173–187, doi:10.1080/10584589508019363.
10. Pandey, D.; Singh, A.K.; Baik, S. Stability of Ferroic Phases in the Highly Piezoelectric Pb(Zr_xTi_{1-x})O_3 Ceramics. *Acta Crystallogr A Found Crystallogr* **2008**, *64*, 192–203, doi:10.1107/S0108767307055511.
11. Wang, K.; Malič, B.; Wu, J. Shifting the Phase Boundary: Potassium Sodium Niobate Derivates. *MRS Bull.* **2018**, *43*, 607–611, doi:10.1557/mrs.2018.178.
12. Wu, J.; Xiao, D.; Zhu, J. Potassium–Sodium Niobate Lead-Free Piezoelectric Materials: Past, Present, and Future of Phase Boundaries. *Chem. Rev.* **2015**, *115*, 2559–2595, doi:10.1021/cr5006809.
13. Wang, Z.; Gu, H.; Hu, Y.; Yang, K.; Hu, M.; Zhou, D.; Guan, J. Synthesis, Growth Mechanism and Optical Properties of (K,Na)NbO_3 Nanostructures. *CrystEngComm* **2010**, *12*, 3157, doi:10.1039/c000169d.
14. Meng, X.; Wang, W.; Ke, H.; Rao, J.; Jia, D.; Zhou, Y. Synthesis, Piezoelectric Property and Domain Behaviour of the Vertically Aligned $K_{1-x}Na_x$ NbO_3 Nanowire with a Morphotropic Phase Boundary. *J. Mater. Chem. C* **2017**, *5*, 747–753, doi:10.1039/C6TC04629K.
15. Jin, W.; Wang, Z.; Li, M.; He, Y.; Hu, X.; Li, L.; Gao, Y.; Hu, Y.; Gu, H.; Wang, X. Evolution of the Composition, Structure, and Piezoelectric Performance of ($K_{1-x}Na_x$)NbO_3 Nanorod Arrays with Hydrothermal Reaction Time. *Appl. Phys. Lett.* **2018**, *112*, 142904, doi:10.1063/1.5021378.
16. Esin, A.A.; Alikin, D.O.; Turygin, A.P.; Abramov, A.S.; Hreščak, J.; Walker, J.; Rojac, T.; Bencan, A.; Malic, B.; Kholkin, A.L.; et al. Dielectric Relaxation and Charged Domain Walls in (K,Na)NbO_3 -Based Ferroelectric Ceramics. *Journal of Applied Physics* **2017**, *121*, 074101, doi:10.1063/1.4975341.
17. Wang, X.; Wu, J.; Xiao, D.; Zhu, J.; Cheng, X.; Zheng, T.; Zhang, B.; Lou, X.; Wang, X. Giant Piezoelectricity in Potassium–Sodium Niobate Lead-Free Ceramics. *J. Am. Chem. Soc.* **2014**, *136*, 2905–2910, doi:10.1021/ja500076h.
18. Ge, W.; Li, J.; Viehland, D.; Chang, Y.; Messing, G.L. Electric-Field-Dependent Phase Volume Fractions and Enhanced Piezoelectricity near the Polymorphic Phase Boundary of $(K_{0.5}Na_{0.5})_{1-x}Li_xNbO_3$ Textured Ceramics. *Phys. Rev. B* **2011**, *83*, 224110, doi:10.1103/PhysRevB.83.224110.
19. Tan, Z.; Xing, J.; Peng, Y.; Zhang, Q.; Zhu, J. Polarization Rotation Boosts Strong Piezoelectric Response in the Lead-Free Perovskite Ferroelectric $K_{0.5}Na_{0.5}NbO_3$. *Phys. Rev. B* **2021**, *104*, 014104, doi:10.1103/PhysRevB.104.014104.
20. Seog, H.J.; Ullah, A.; Ahn, C.W.; Kim, I.W.; Lee, S.Y.; Park, J.; Lee, H.J.; Won, S.S.; Kim, S.H. Recent Progress in Potassium Sodium Niobate Lead-Free Thin Films. *J. Korean Phys. Soc.* **2018**, *72*, 1467–1483, doi:10.3938/jkps.72.1467.
21. von Helden, L.; Bogula, L.; Janolin, P.E.; Hanke, M.; Breuer, T.; Schmidbauer, M.; Ganschow, S.; Schwarzkopf, J. Huge Impact of Compressive Strain on Phase Transition Temperatures in Epitaxial Ferroelectric $K_xNa_{1-x}NbO_3$ Thin Films. *Appl. Phys. Lett.* **2019**, *114*, 232905, doi:10.1063/1.5094405.
22. Shan, D.L.; Lei, C.H.; Cai, Y.C.; Pan, K.; Liu, Y.Y. Mechanical Control of Electrocaloric Response in Epitaxial Ferroelectric Thin Films. *International Journal of Solids and Structures* **2021**, *216*, 59–67, doi:10.1016/j.ijsolstr.2021.01.020.
23. Liu, Y.Y.; Vasudevan, R.K.; Pan, K.; Xie, S.H.; Liang, W.I.; Kumar, A.; Jesse, S.; Chen, Y.C.; Chu, Y.H.; Nagarajan, V.; et al. Controlling Magnetoelectric Coupling by Nanoscale Phase Transformation in Strain Engineered Bismuth Ferrite. *Nanoscale* **2012**, *4*, 3175, doi:10.1039/c2nr00039c.
24. Wang, J.J.; Su, Y.J.; Wang, B.; Ouyang, J.; Ren, Y.H.; Chen, L.Q. Strain Engineering of Dischargeable Energy Density of Ferroelectric Thin-Film Capacitors. *Nano Energy* **2020**, *72*, 104665, doi:10.1016/j.nanoen.2020.104665.

25. Liu, D.; Bai, G.; Gao, C. Phase Diagrams Classification Based on Machine Learning and Phenomenological Investigation of Physical Properties in $K_{1-x}Na_xNbO_3$ Thin Films. *Journal of Applied Physics* **2020**, *127*, 154101, doi:10.1063/5.0004167.
26. Zhou, M.J.; Wang, J.J.; Chen, L.Q.; Nan, C.W. Strain, Temperature, and Electric-Field Effects on the Phase Transition and Piezoelectric Responses of $K_{0.5}Na_{0.5}NbO_3$ Thin Films. *Journal of Applied Physics* **2018**, *123*, 154106, doi:10.1063/1.5027505.
27. Pohlmann, H.; Wang, J.J.; Wang, B.; Chen, L.Q. A Thermodynamic Potential and the Temperature-Composition Phase Diagram for Single-Crystalline $K_{1-x}Na_xNbO_3$($0 \leq x \leq 0.5$). *Appl. Phys. Lett.* **2017**, *110*, 102906, doi:10.1063/1.4978360.
28. Peng, J.; Shan, D.; Liu, Y.; Pan, K.; Lei, C.; He, N.; Zhang, Z.; Yang, Q. A Thermodynamic Potential for Barium Zirconate Titanate Solid Solutions. *npj Comput Mater* **2018**, *4*, 66, doi:10.1038/s41524-018-0126-3.
29. Liu, Y.Y.; Zhu, Z.X.; Li, J.F.; Li, J.Y. Misfit Strain Modulated Phase Structures of Epitaxial $Pb(Zr_{1-x}Ti_x)O_3$ Thin Films: The Effect of Substrate and Film Thickness. *Mechanics of Materials* **2010**, *42*, 816–826, doi:10.1016/j.mechmat.2010.06.002.
30. Pertsev, N.A.; Zembilgotov, A.G.; Tagantsev, A.K. Effect of Mechanical Boundary Conditions on Phase Diagrams of Epitaxial Ferroelectric Thin Films. *Phys. Rev. Lett.* **1998**, *80*, 1988–1991, doi:10.1103/PhysRevLett.80.1988.
31. Liu, Y.Y.; Li, J.Y. Shear-Driven Morphotropic Phase Boundary in Epitaxial Ferroelectric Thin Films. *Phys. Rev. B* **2011**, *84*, 132104, doi:10.1103/PhysRevB.84.132104.
32. Haun, M.J.; Furman, E.; Jang, S.J.; Cross, L.E. Thermodynamic Theory of the Lead Zirconate-Titanate Solid Solution System, Part I: Phenomenology. *Ferroelectrics* **1989**, *99*, 13–25, doi:10.1080/00150198908221436.
33. Liu, Y.Y.; Yang, L.; Li, J.Y. Strain-Engineered Orthorhombic-Rhombohedral Phase Boundary in Epitaxial Bismuth Ferrite Films. *Journal of Applied Physics* **2013**, *113*, 183524, doi:10.1063/1.4804962.
34. Pertsev, N.A.; Kukhar, V.G.; Kohlstedt, H.; Waser, R. Phase Diagrams and Physical Properties of Single-Domain Epitaxial $Pb(Zr_{1-x}Ti_x)O_3$ Thin Films. *Phys. Rev. B* **2003**, *67*, 054107, doi:10.1103/PhysRevB.67.054107.
35. Tomeno, I.; Tsunoda, Y.; Oka, K.; Matsuura, M.; Nishi, M. Lattice Dynamics of Cubic $NaNbO_3$: An Inelastic Neutron Scattering Study. *Phys. Rev. B* **2009**, *80*, 104101, doi:10.1103/PhysRevB.80.104101.
36. Liang, L.; Li, Y.L.; Chen, L.Q.; Hu, S.Y.; Lu, G.H. A Thermodynamic Free Energy Function for Potassium Niobate. *Applied Physics Letters* **2009**, *94*, 072904, doi:10.1063/1.3081418.
37. Barman, A.; Kar-Narayan, S.; Mukherjee, D. Caloric Effects in Perovskite Oxides. *Adv. Mater. Interfaces* **2019**, *6*, 1900291, doi:10.1002/admi.201900291.
38. Shan, D.; Pan, K.; Liu, Y.; Li, J. High Fidelity Direct Measurement of Local Electrocaloric Effect by Scanning Thermal Microscopy. *Nano Energy* **2020**, *67*, 104203, doi:10.1016/j.nanoen.2019.104203.
39. Pirc, R.; Kutnjak, Z.; Blinc, R.; Zhang, Q.M. Electrocaloric Effect in Relaxor Ferroelectrics. *Journal of Applied Physics* **2011**, *110*, 074113, doi:10.1063/1.3650906.
40. He, N.; Li, Q.; Lei, C.; Pan, J.; Shan, D.; Pan, K.; Liu, Y. Electrocaloric Response Modulated by Misfit Strain in Different Oriented Epitaxial Ferroelectric Thin Films. *International Journal of Solids and Structures* **2022**, *252*, 111808, doi:10.1016/j.ijsolstr.2022.111808.
41. Shan, D.; Cai, Y.; Lei, C.; Peng, J.; He, N.; Pan, K.; Liu, Y.; Li, J. Electric-Field-Driven Coexistence of Positive and Negative Electrocaloric Effects near Room Temperature for High-Efficiency Two-Stage Cooling. *Appl. Phys. Lett.* **2021**, *118*, 122905, doi:10.1063/5.0047020.
42. Lei, C.H.; Liu, Y. Correlations between Local Electrocaloric Effect and Domains in Ferroelectric Crystals. *Appl. Phys. Lett.* **2022**, *121*, 102902, doi:10.1063/5.0094473.
43. Luo, J.; Sun, W.; Zhou, Z.; Lee, H.Y.; Wang, K.; Zhu, F.; Bai, Y.; Wang, Z.J.; Li, J.-F. Monoclinic (K,Na)NbO_3 Ferroelectric Phase in Epitaxial Films. *Adv. Electron. Mater.* **2017**, *3*, 1700226, doi:10.1002/aelm.201700226.